Atmospheric Dynamics

the CAM-FV dynamical core

Peter Hjort Lauritzen

Atmospheric Modeling and Predictability Section
Climate and Global Dynamics Division
National Center for Atmospheric Research

Community Atmosphere Model (CAM) Tutorial
NCAR's Mesa Lab
July 27-31, 2009.

'Definition' of an atmospheric dynamical core

'Roughly speaking, the **dynamical core** solves the governing fluid and thermodynamic equations on resolved scales, while the parameterizations represent sub-grid-scale processes and other processes not included in the dynamical core such as radiative transfer.' - Thuburn (2008)

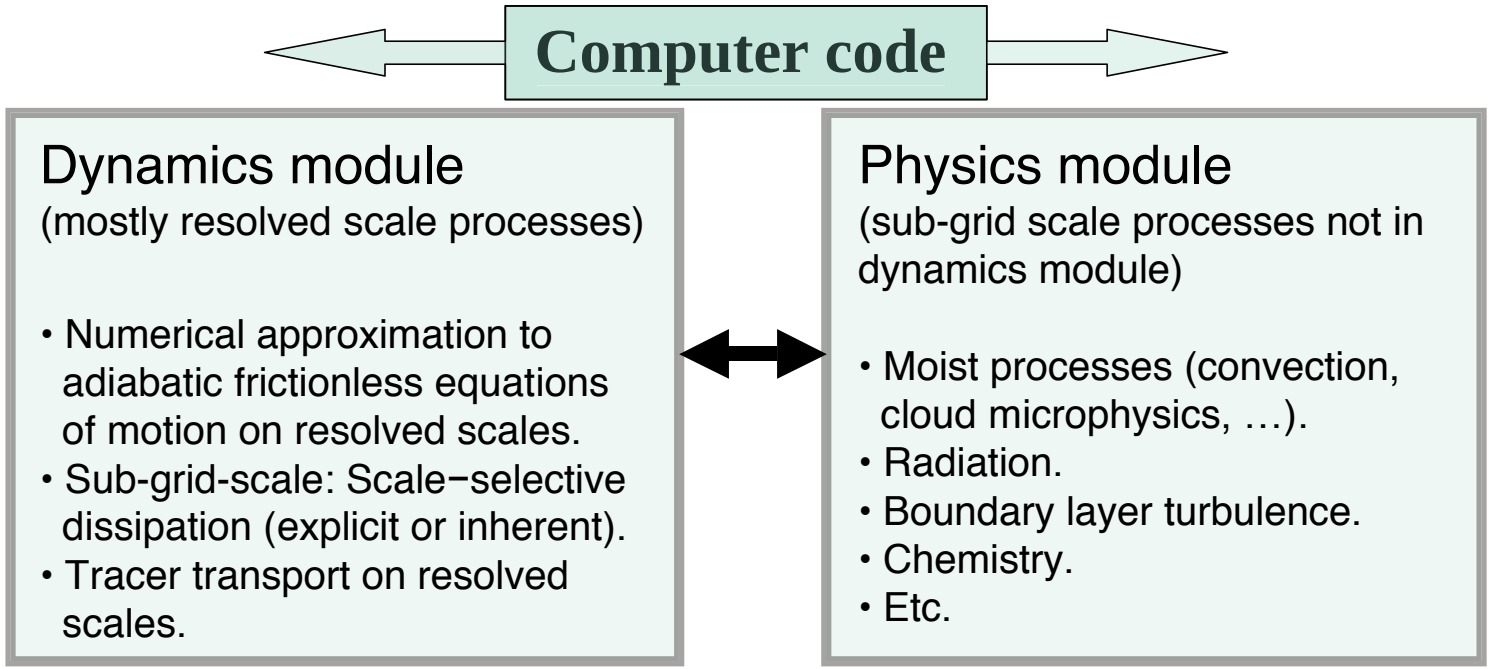

‘Definition’ of an atmospheric dynamical core

Define:

- Adiabatic frictionless equations of motion
- Horizontal and vertical discretization grid

Spherical (horizontal) discretization grid

CAM-FV uses regular latitude-longitude grid:

- Horizontal position: (λ, θ), where λ longitude and θ latitude.
- Horizontal resolution specified in `configure` as:

$$\texttt{-res}\ \Delta\lambda \times \Delta\theta$$

where, e.g., $\Delta\lambda \times \Delta\theta = 1.9 \times 2.5$ corresponding to `nlon=144`, `nlat=96`. Changing resolution requires a 're-compile' and forcing datasets at the desired resolution.

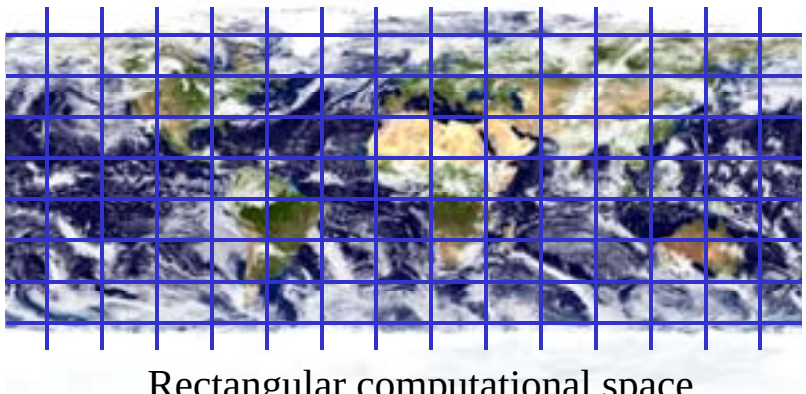

Rectangular computational space

Vertical coordinate

- CAM-FV uses a Lagrangian ('floating') vertical coordinate ς so that

$$\frac{d\varsigma}{dt} = 0,$$

i.e. vertical surfaces are material surfaces (no flow across them).

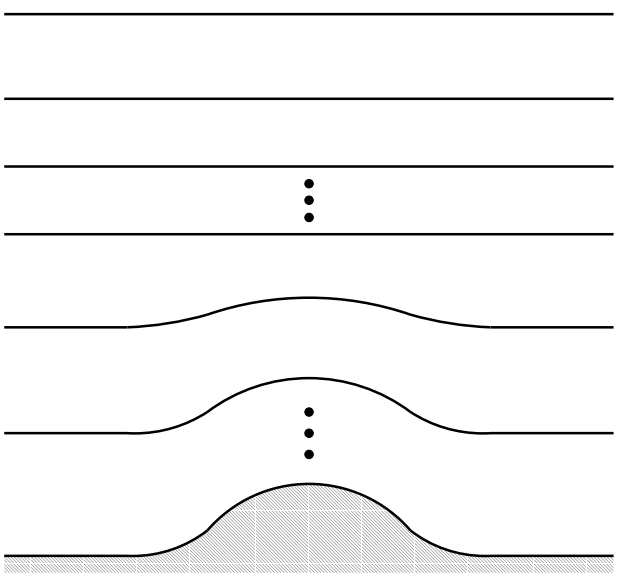

Figure shows 'usual' terrain-following vertical coordinate $\eta(p_s, p)$ (where p_s is surface pressure):

- $\eta(p_s, p)$ is a monotonic function of p.
- $\eta(p_s, p_s) = 1$
- $\eta(p_s, 0) = 0$
- $\eta(p_s, p_{top}) = \eta_{top}$.

Boundary conditions are:

- $\frac{d\eta(p_s, p_s)}{dt} = 0$
- $\frac{d\eta(p_s, p_{top})}{dt} = \omega(p_{top}) = 0$

(ω is vertical velocity in pressure coordinates)

Vertical coordinate

- CAM-FV uses a Lagrangian ('floating') vertical coordinate ς so that

$$\frac{d\varsigma}{dt} = 0,$$

i.e. vertical surfaces are material surfaces (no flow across them).

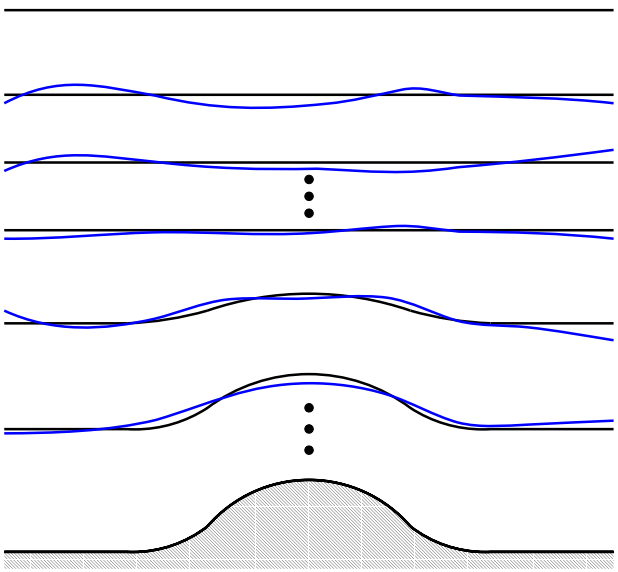

Figure:

- Set $\varsigma = \eta$ at time t_{start} (black lines).
- For $t > t_{start}$ the vertical levels deform as they move with the flow (blue lines).
- To avoid excessive deformation of the vertical levels (non-uniform vertical resolution) the prognostic variables defined in the Lagrangian layers ς are periodically remapped (= conservative interpolation) back to the Eulerian reference coordinates η (more on this later).

Vertical coordinate

- Vertical resolution specified in `configure` as:

  `-nlev` *klev*

  where *klev* is the number of vertical levels, e.g., *klev* $= 26$ or *klev* $= 30$. Changing vertical resolution requires a 're-compile'.

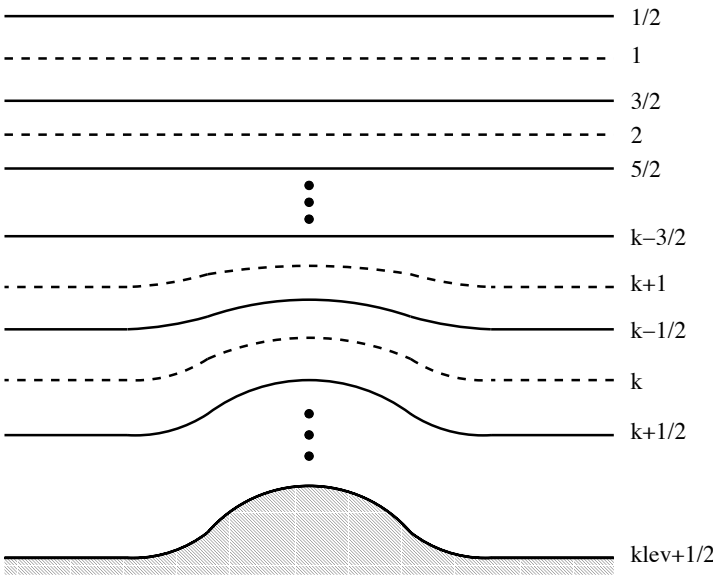

Figure: 'Center' of a layer is referred to as a 'full' level and referenced with an integer value k. Layer k is bounded by 'half' levels $k \pm 1/2$.

Adiabatic frictionless equations of motion

The following approximations are made to the compressible Euler equations:

- **Spherical geoid**: Geopotential Φ is only a function of radial distance from the center of the Earth r: $\Phi = \Phi(r)$ (for planet Earth the true gravitational acceleration is much stronger than the centrifugal force).

Adiabatic frictionless equations of motion

The following approximations are made to the compressible Euler equations:

- **Spherical geoid**: Geopotential Φ is only a function of radial distance from the center of the Earth r: $\Phi = \Phi(r)$ (for planet Earth the true gravitational acceleration is much stronger than the centrifugal force).
- **Hydrostatic approximation**: Ignore the acceleration term in the vertical component of the momentum equations so that it reads:

$$g = -\rho \frac{\partial p}{\partial z}, \tag{1}$$

where g gravity, ρ density and p pressure. Good approximation down to horizontal scales greater than approximately $10km$.

Adiabatic frictionless equations of motion

The following approximations are made to the compressible Euler equations:

- **Spherical geoid**: Geopotential Φ is only a function of radial distance from the center of the Earth r: $\Phi = \Phi(r)$ (for planet Earth the true gravitational acceleration is much stronger than the centrifugal force).
- **Hydrostatic approximation**: Ignore the acceleration term in the vertical component of the momentum equations so that it reads:

$$g = -\rho \frac{\partial p}{\partial z}, \tag{1}$$

  where g gravity, ρ density and p pressure. Good approximation down to horizontal scales greater than approximately $10km$.
- **Shallow atmosphere**: A collection of approximations. Coriolis terms involving the horizontal components of Ω are neglected (Ω is angular velocity), factors $1/r$ are replaced with $1/a$ where a is the mean radius of the Earth and certain other metric terms are neglected so that the system retains conservation laws for energy and angular momentum.

Adiabatic frictionless equations of motion using Lagrangian vertical coordinates

Assuming a Lagrangian vertical coordinate the hydrostatic equations of motion integrated over a layer can be written as

$$\begin{aligned}
\text{mass air:} \quad & \frac{\partial(\delta p)}{\partial t} = -\nabla_h \cdot (\vec{v}_h \delta p)\,, \\
\text{mass tracers:} \quad & \frac{\partial(\delta p q)}{\partial t} = -\nabla_h \cdot (\vec{v}_h\, q \delta p)\,, \\
\text{horizontal momentum:} \quad & \frac{\partial \vec{v}_h}{\partial t} = -\left(\zeta + f\right) \vec{k} \times \vec{v}_h - \nabla_h \kappa - \nabla_p \Phi, \\
\text{thermodynamic:} \quad & \frac{\partial(\delta p \Theta)}{\partial t} = -\nabla_h \cdot (\vec{v}_h \delta p \Theta)
\end{aligned}$$

where δp is the layer thickness, $\vec{v}_h$ is horizontal wind, q tracer mixing ratio, ζ vorticity, f Coriolis, κ kinetic energy, Θ potential temperature. The momentum equations are written in vector invariant form.

Adiabatic frictionless equations of motion using Lagrangian vertical coordinates

Assuming a Lagrangian vertical coordinate the hydrostatic equations of motion integrated over a layer can be written as

$$\begin{aligned}
\text{mass air:} \qquad & \frac{\partial(\delta p)}{\partial t} = -\nabla_h \cdot (\vec{v}_h \delta p)\,, \\
\text{mass tracers:} \qquad & \frac{\partial(\delta p q)}{\partial t} = -\nabla_h \cdot (\vec{v}_h\, q \delta p)\,, \\
\text{horizontal momentum:} \qquad & \frac{\partial \vec{v}_h}{\partial t} = -\left(\zeta + f\right) \vec{k} \times \vec{v}_h - \nabla_h \kappa - \nabla_p \Phi, \\
\text{thermodynamic:} \qquad & \frac{\partial(\delta p \Theta)}{\partial t} = -\nabla_h \cdot (\vec{v}_h \delta p \Theta)
\end{aligned}$$

The equations of motion are discretized using an Eulerian finite-volume approach.

Finite-volume discretization of continuity equation

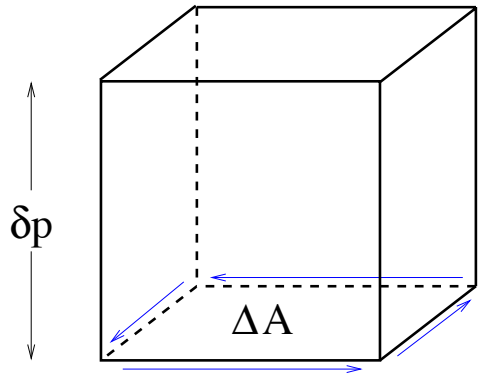

Integrate the flux-form continuity equation horizontally over a control volume:

$$\frac{\partial}{\partial t}\iint_A \delta p\, dA = -\iint_A \nabla_h \left(\vec{v}_h \delta p\right)\, dA, \tag{2}$$

where A is the horizontal extent of the control volume. Using Gauss's divergence theorem for the right-hand side of (2) we get:

$$\frac{\partial}{\partial t}\iint_A \delta p\, dA = -\oint_{\partial A} \delta p\, \vec{v}\cdot\vec{n}\, dA, \tag{3}$$

where ∂A is the boundary of A and $\vec{n}$ is outward pointing normal unit vector of ∂A.

Finite-volume discretization of continuity equation

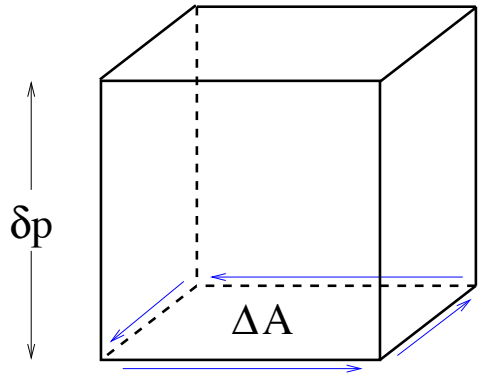

Integrate the flux-form continuity equation horizontally over a control volume:

$$\frac{\partial}{\partial t}\iint_A \delta p \, dA = -\iint_A \nabla_h \left(\vec{v}_h \delta p\right) \, dA, \tag{2}$$

where A is the horizontal extent of the control volume. Using Gauss's divergence theorem for the right-hand side of (2) we get:

$$\frac{\partial}{\partial t}\iint_A \delta p \, dA = -\oint_{\partial A} \delta p \, \vec{v} \cdot \vec{n} \, dA, \tag{3}$$

Right-hand side of (3) represents the instantaneous flux of mass through the vertical faces of the control volume.

Finite-volume discretization of continuity equation

$$\frac{\partial}{\partial t}\iint_A \delta p \, dA = -\oint_{\partial A} \delta p \, \vec{v}\cdot\vec{n}\, dA. \tag{4}$$

Discretize (4) in space

$$\Delta A \frac{\partial \overline{\delta p}}{\partial t} = -\sum_{f=1}^{4} \left[\langle \delta p \vec{v}\rangle \cdot \vec{n}\Delta\ell\right]_f, \tag{5}$$

where

- $\overline{\delta}p =$ horizontal mean value of δp
- $\vec{n}_f =$ unit vector normal to the fth cell face pointing outward
- $\Delta\ell_f$ is the length of the face in question
- $\vec{v}_f =$ instantaneous values of $\vec{v}$ at the cell face f
- brackets represent averages in either λ or θ direction over the cell face.

Finite-volume discretization of continuity equation

$$\frac{\partial}{\partial t}\iint_A \delta p \, dA = -\oint_{\partial A} \delta p \, \vec{v}\cdot\vec{n}\, dA. \tag{4}$$

Discretize (4) in space

$$\Delta A \frac{\partial \overline{\delta p}}{\partial t} = -\sum_{f=1}^{4} \left[\langle \delta p \vec{v}\rangle \cdot \vec{n}\Delta\ell\right]_f , \tag{5}$$

and integrate (5) over the time-step Δt_{dyn}

$$\Delta A\, \overline{\delta p}^{n+1} = \Delta A\, \overline{\delta p}^{n} - \Delta t_{dyn} \sum_{f=1}^{4} \left[\overline{\overline{\langle \delta p \vec{v}\rangle}} \cdot \vec{n}\Delta\ell\right]_f , \tag{6}$$

where n is the time-level index and the double-bar refers to the time average over Δt_{dyn}.

Each term in the sum on the right-hand side of (6) represents the mass transported through one of the four vertical control volume faces into the cell during one time-step (graphical illustration on next page).

Finite-volume discretization of continuity equation: Tracking mass

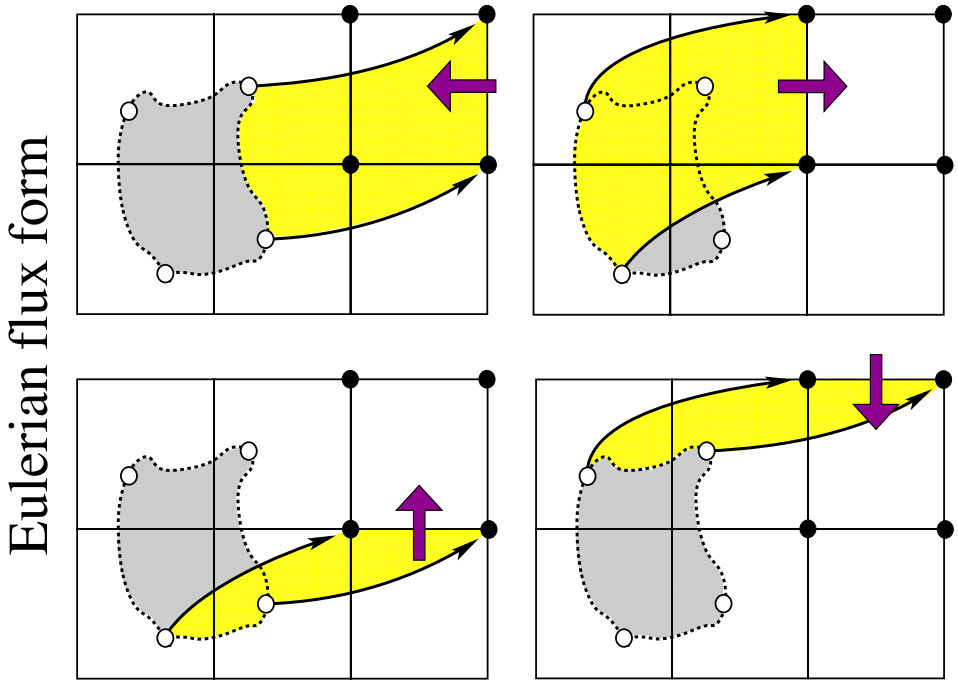

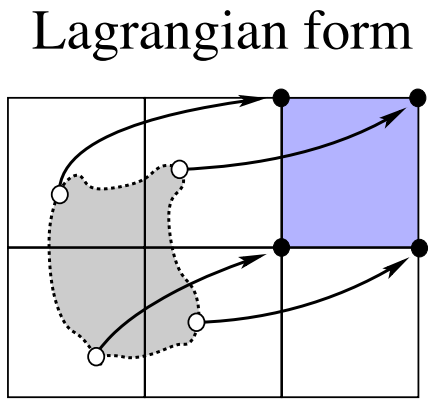

The yellow areas are 'swept' through the control volume faces during one time-step. The grey area is the corresponding Lagrangian area (area moving with the flow with no flow through its boundaries that ends up at the Eulerian control volume after one time-step). Black arrows show parcel trajectories.

Note that adding up the yellow areas results in the grey area!

Finite-volume discretization of continuity equation: Tracking mass

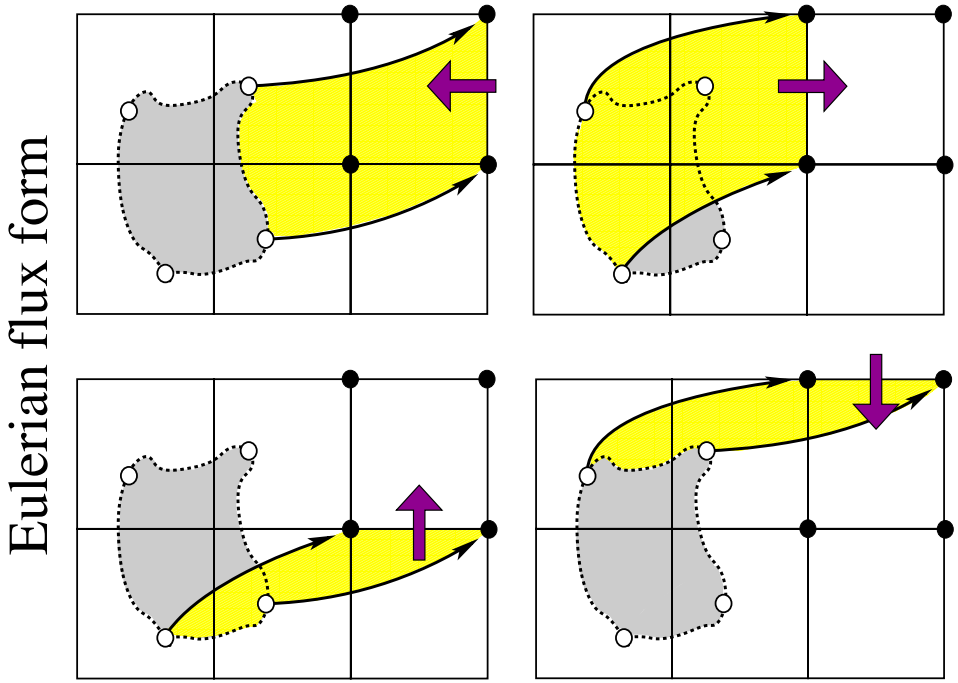

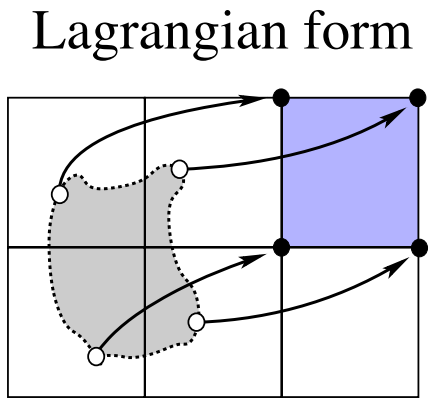

Until now everything has been exact. How do we approximate the fluxes numerically?

- In CAM-FV the Lin and Rood (1996) scheme is used which is a dimensionally split scheme (that is, rather than estimating the boundaries of the yellow areas and integrate over them, fluxes are estimated by successive applications of one-dimensional operators in each coordinate direction).

Finite-volume discretization of continuity equation: Tracking mass

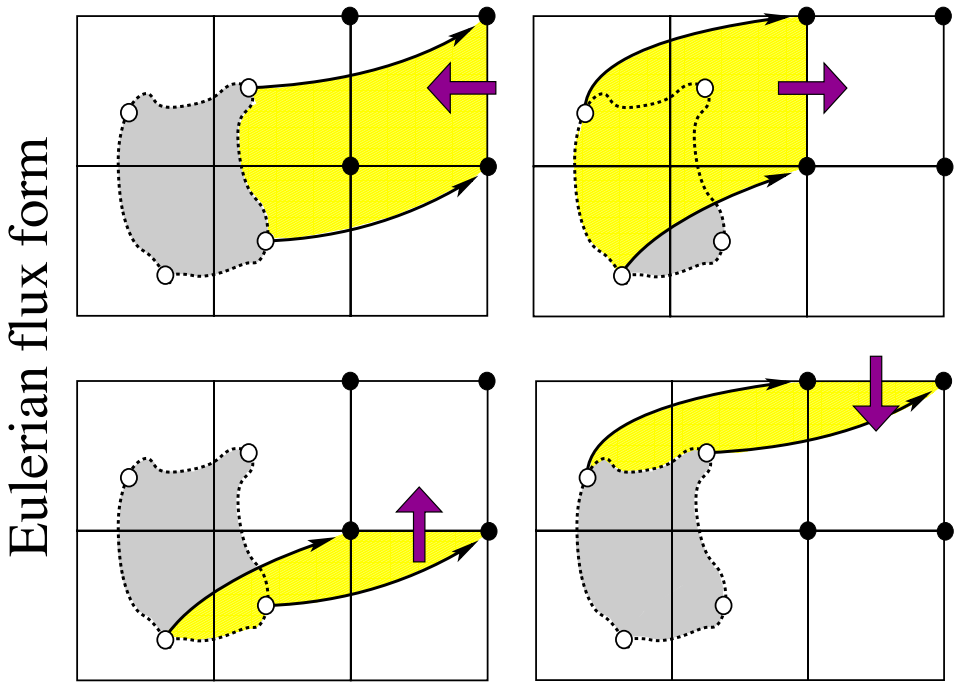

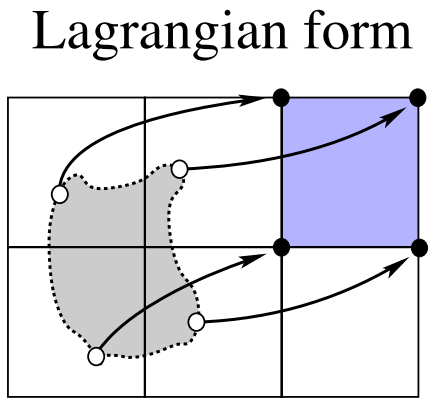

Until now everything has been exact. How do we approximate the fluxes numerically?

- (before showing equations for Lin and Rood (1996) scheme) What is the effective Lagrangian area associated with the Lin and Rood (1996) scheme?

Finite-volume discretization of continuity equation: Tracking mass

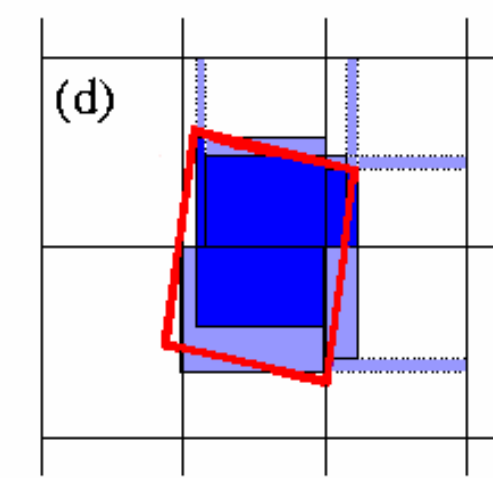

Figure: Red lines define boundary of exact Lagrangian cell for a special case with deformational, rotational and divergent wind field. Blue colors is Lagrangian cell associated with the Lin and Rood (1996) scheme. Dark blue shading weights integrated mass with 1 and light blue shading weights integrated mass with 1/2. See Machenhauer et al. (2009) for details.

Until now everything has been exact. How do we approximate the fluxes numerically?

- (before showing equations for Lin and Rood (1996) scheme) What is the effective Lagrangian area associated with the Lin and Rood (1996) scheme?

The Lin and Rood (1996) advection scheme

$$\overline{\delta p}^{n+1} = \overline{\delta p}^{n} + F^{\lambda}\left[\tfrac{1}{2}\left(\overline{\delta p}^{n} + f^{\theta}(\overline{\delta p}^{n})\right)\right] + F^{\theta}\left[\tfrac{1}{2}\left(\overline{\delta p}^{n} + f^{\lambda}(\overline{\delta p}^{n})\right)\right],$$

where

$$F^{\lambda,\theta} = \text{ flux divergence in } \lambda \text{ or } \theta \text{ coordinate direction}$$

$$f^{\lambda,\theta} = \text{ advective update in } \lambda \text{ or } \theta \text{ coordinate direction}$$

The Lin and Rood (1996) advection scheme

$$\overline{\delta p}^{n+1} = \overline{\delta p}^{n} + F^{\lambda}\left[\frac{1}{2}\left(\overline{\delta p}^{n} + f^{\theta}(\overline{\delta p}^{n})\right)\right] + F^{\theta}\left[\frac{1}{2}\left(\overline{\delta p}^{n} + f^{\lambda}(\overline{\delta p}^{n})\right)\right],$$

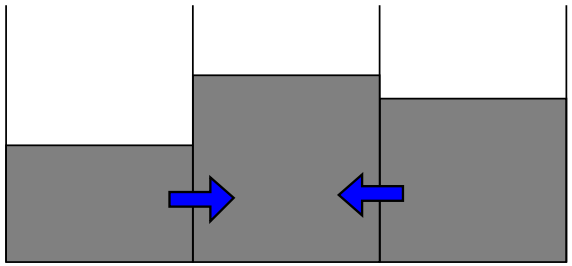

- Figure: Graphical illustration of flux-divergence operator F^{λ}. Shaded areas show cell average values for the cell we wish to make a forecast for and the two adjacent cells.

The Lin and Rood (1996) advection scheme

$$\overline{\delta p}^{n+1} = \overline{\delta p}^{n} + F^{\lambda}\left[\frac{1}{2}\left(\overline{\delta p}^{n} + f^{\theta}(\overline{\delta p}^{n})\right)\right] + F^{\theta}\left[\frac{1}{2}\left(\overline{\delta p}^{n} + f^{\lambda}(\overline{\delta p}^{n})\right)\right],$$

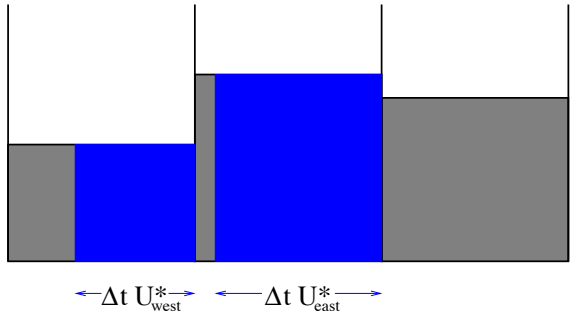

- $u^{*}_{east\,/\,west}$ are the time-averaged winds on each face (more on how these are obtained later).
- F^{λ} is proportional to the difference between mass 'swept' through east and west cell face.
- $f^{\lambda} = F^{\lambda} + \overline{\overline{<\delta p>}}\Delta t_{dyn} D$, where D is divergence.
- On Figure we assume constant sub-grid-cell reconstructions for the fluxes.

The Lin and Rood (1996) advection scheme

$$\overline{\delta p}^{n+1} = \overline{\delta p}^{n} + F^{\lambda}\left[\frac{1}{2}\left(\overline{\delta p}^{n} + f^{\theta}(\overline{\delta p}^{n})\right)\right] + F^{\theta}\left[\frac{1}{2}\left(\overline{\delta p}^{n} + f^{\lambda}(\overline{\delta p}^{n})\right)\right],$$

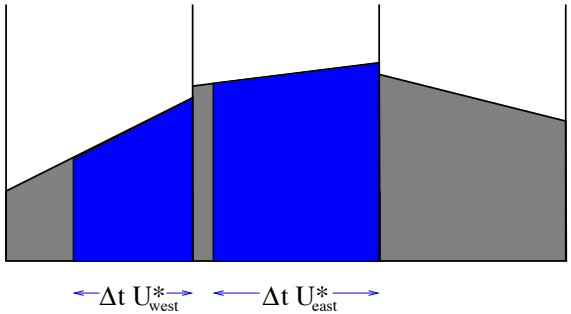

Higher-order approximation to the fluxes:

- Piecewise linear sub-grid-scale reconstruction (van Leer, 1977): Fit a linear function using neighboring grid-cell average values with mass-conservation as a constraint (i.e. area under linear function = cell average.).

The Lin and Rood (1996) advection scheme

$$\overline{\delta p}^{n+1} = \overline{\delta p}^{n} + F^{\lambda}\left[\frac{1}{2}\left(\overline{\delta p}^{n} + f^{\theta}(\overline{\delta p}^{n})\right)\right] + F^{\theta}\left[\frac{1}{2}\left(\overline{\delta p}^{n} + f^{\lambda}(\overline{\delta p}^{n})\right)\right],$$

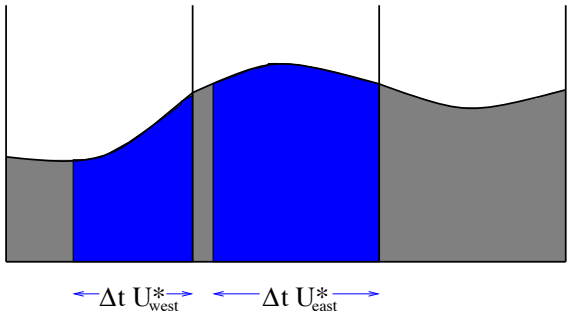

Higher-order approximation to the fluxes:

- Piecewise linear sub-grid-scale reconstruction (van Leer, 1977): Fit a linear function using neighboring grid-cell average values with mass-conservation as a constraint (i.e. area under linear function = cell average.).
- Piecewise parabolic sub-grid-scale reconstruction (Colella and Woodward, 1984): Fit parabola using neighboring grid-cell average values with mass-conservation as a constraint. Note: Reconstruction is C^0 across cell edges.

The Lin and Rood (1996) advection scheme

$$\overline{\delta p}^{n+1} = \overline{\delta p}^{n} + F^{\lambda}\left[\frac{1}{2}\left(\overline{\delta p}^{n} + f^{\theta}(\overline{\delta p}^{n})\right)\right] + F^{\theta}\left[\frac{1}{2}\left(\overline{\delta p}^{n} + f^{\lambda}(\overline{\delta p}^{n})\right)\right],$$

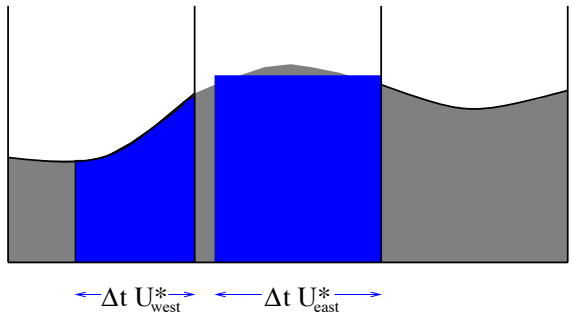

Higher-order approximation to the fluxes:

- Piecewise linear sub-grid-scale reconstruction (van Leer, 1977): Fit a linear function using neighboring grid-cell average values with mass-conservation as a constraint (i.e. area under linear function = cell average.).
- Piecewise parabolic sub-grid-scale reconstruction (Colella and Woodward, 1984): Fit parabola using neighboring grid-cell average values with mass-conservation as a constraint. Note: Reconstruction is continuous at cell edges.
- Reconstruction function may 'over'- or 'undershoot' which may lead to unphysical and/or oscillatory solutions. Use limiters to render reconstruction function monotone.

The Lin and Rood (1996) advection scheme

$$\overline{\delta p}^{n+1} = \overline{\delta p}^{n} + F^{\lambda}\left[\frac{1}{2}\left(\overline{\delta p}^{n} + f^{\theta}(\overline{\delta p}^{n})\right)\right] + F^{\theta}\left[\frac{1}{2}\left(\overline{\delta p}^{n} + f^{\lambda}(\overline{\delta p}^{n})\right)\right],$$

Advantages:

- Inherently mass conservative.
- Formulated in terms of one-dimensional operators.
- Preserves a constant for a non-divergent flow field (if the finite-difference approximation to divergence is zero).
- Preserves linear correlations between trace species (if monotonicity filters are not applied)
- Has monotone options.

Namelist variables for *outer* operators

IORD: Scheme used for F^{λ}, JORD: Scheme used for F^{θ}

Options for sub-grid-scale reconstruction (IORD, JORD = -2,1,2,3,4,5,6):

-2. Piecewise linear (non-monotone), (van Leer, 1977).
1. Piecewise constant (Godunov, 1959).
2. Piecewise linear with monotonicity constraint (van Leer, 1977).
3. Piecewise parabolic with monotonicity constraint (Colella and Woodward, 1984).
4. Piecewise parabolic with monotonicity constraint (Lin and Rood, 1996).
5. Piecewise parabolic with positive definite constraint (Lin and Rood, 1996).
6. Piecewise parabolic with quasi-monotone constraint (Lin and Rood, 1996).

Defaults: IORD=JORD=4

Namelist variables for *outer* operators

- In top layers operators are reduced to first order:

  if (k$\leq$klev/8) IORD=JORD=1

  E.g., for klev=30 the operators are altered in the top 3 layers.

- The advective $f^{\lambda,\theta}$ (*inner*) operators are 'hard-coded' to 1st order. For a linear analysis of the consequences of using *inner* and *outer* operators of different orders see Lauritzen (2007).

Adiabatic frictionless equations of motion

Hydrostatic equations of motion integrated over a Lagrangian layer

$$
\begin{aligned}
\frac{\partial(\delta p)}{\partial t} &= -\nabla_h \cdot (\vec{v}_h \delta p)\,, \\
\frac{\partial(\delta p q)}{\partial t} &= -\nabla_h \cdot (\vec{v}_h \delta p)\,, \\
\frac{\partial \vec{v}_h}{\partial t} &= -\left(\zeta + f\right)\vec{k} \times \vec{v}_h - \nabla_h \kappa - \nabla_p \Phi, \\
\frac{\partial(\delta p \Theta)}{\partial t} &= -\nabla_h \cdot (\vec{v}_h \delta p \Theta)
\end{aligned}
$$

The equations of motion are discretized using an Eulerian finite-volume approach.

Adiabatic frictionless equations of motion

Hydrostatic equations of motion integrated over a Lagrangian layer

$$
\begin{aligned}
\overline{\delta p}^{n+1} &= \overline{\delta p}^{n} + F^{\lambda}\left[\frac{1}{2}\left(\overline{\delta p}^{n} + f^{\theta}(\overline{\delta p}^{n})\right)\right] + F^{\theta}\left[\frac{1}{2}\left(\overline{\delta p}^{n} + f^{\lambda}(\overline{\delta p}^{n})\right)\right], \\
\frac{\partial(\delta p q)}{\partial t} &= -\nabla_h \cdot (\vec{v}_h \delta p)\,, \\
\frac{\partial \vec{v}_h}{\partial t} &= -(\zeta + f)\,\vec{k} \times \vec{v}_h - \nabla_h \kappa - \nabla_p \Phi, \\
\frac{\partial(\delta p \Theta)}{\partial t} &= -\nabla_h \cdot (\vec{v}_h \delta p \Theta)
\end{aligned}
$$

Adiabatic frictionless equations of motion

Hydrostatic equations of motion integrated over a Lagrangian layer

$$
\begin{aligned}
\overline{\delta p}^{n+1} &= \overline{\delta p}^{n} + F^{\lambda}\left[\frac{1}{2}\left(\overline{\delta p}^{n} + f^{\theta}(\overline{\delta p}^{n})\right)\right] + F^{\theta}\left[\frac{1}{2}\left(\overline{\delta p}^{n} + f^{\lambda}(\overline{\delta p}^{n})\right)\right], \\
\overline{\delta pq}^{n+1} &= \text{sub-cycled (discussed later)}, \\
\frac{\partial \vec{v}_h}{\partial t} &= -\left(\zeta + f\right)\vec{k} \times \vec{v}_h - \nabla_h \kappa - \nabla_p \Phi, \\
\frac{\partial(\delta p \Theta)}{\partial t} &= -\nabla_h \cdot (\vec{v}_h \delta p \Theta)
\end{aligned}
$$

Adiabatic frictionless equations of motion

Hydrostatic equations of motion integrated over a Lagrangian layer

$$
\begin{aligned}
\overline{\delta p}^{n+1} &= \overline{\delta p}^{n} + F^{\lambda}\left[\frac{1}{2}\left(\overline{\delta p}^{n} + f^{\theta}(\overline{\delta p}^{n})\right)\right] + F^{\theta}\left[\frac{1}{2}\left(\overline{\delta p}^{n} + f^{\lambda}(\overline{\delta p}^{n})\right)\right], \\
\overline{\delta p q}^{n+1} &= \text{sub-cycled (discussed later)}, \\
\vec{v}_h^{\,n+1} &= \vec{v}_h^{\,n} - \vec{\Gamma}^1\left[(\zeta + f)\,\vec{k} \times \vec{v}_h\right] - \nabla_h\left(\vec{\Gamma}^2 \kappa\right) - \Delta t_{dyn} \widehat{P}, \\
\frac{\partial(\delta p \Theta)}{\partial t} &= -\nabla_h \cdot (\vec{v}_h \delta p \Theta)
\end{aligned}
$$

- $\vec{\Gamma}^1$ is operator using combinations of $F^{\lambda,\theta}$ and $f^{\lambda,\theta}$ as components to approximate the time-volume-average of the vertical component of absolute vorticity. Similarly for $\vec{\Gamma}^2$ but for kinetic energy. ∇_h is simply approximated by finite differences. For details see Lin (2004).
- $\widehat{P}$ is a finite-volume discretization of the pressure gradient force (see Lin 1997 for details).

Adiabatic frictionless equations of motion

Hydrostatic equations of motion integrated over a Lagrangian layer

$$
\begin{aligned}
\overline{\delta p}^{n+1} &= \overline{\delta p}^{n} + F^{\lambda}\left[\frac{1}{2}\left(\overline{\delta p}^{n} + f^{\theta}(\overline{\delta p}^{n})\right)\right] + F^{\theta}\left[\frac{1}{2}\left(\overline{\delta p}^{n} + f^{\lambda}(\overline{\delta p}^{n})\right)\right], \\
\overline{\delta pq}^{n+1} &= \text{sub-cycled (discussed later)}, \\
\vec{v}_h^{n+1} &= \vec{v}_h^{n} - \vec{\Gamma}^{1}\left[(\zeta + f)\,\vec{k} \times \vec{v}_h\right] - \nabla_h\left(\vec{\Gamma}^{2}\kappa\right) - \Delta t_{dyn}\widehat{P}, \\
\overline{\Theta\delta p}^{n+1} &= \overline{\Theta\delta p}^{n} + F^{\lambda}\left[\frac{1}{2}\left(\overline{\Theta\delta p}^{n} + f^{\theta}(\overline{\Theta\delta p}^{n})\right)\right] + F^{\theta}\left[\frac{1}{2}\left(\overline{\Theta\delta p}^{n} + f^{\lambda}(\overline{\Theta\delta p}^{n})\right)\right],
\end{aligned}
$$

Adiabatic frictionless equations of motion

Hydrostatic equations of motion integrated over a Lagrangian layer

$$
\begin{aligned}
\overline{\delta p}^{n+1} &= \overline{\delta p}^{n} + F^{\lambda}\left[\frac{1}{2}\left(\overline{\delta p}^{n} + f^{\theta}(\overline{\delta p}^{n})\right)\right] + F^{\theta}\left[\frac{1}{2}\left(\overline{\delta p}^{n} + f^{\lambda}(\overline{\delta p}^{n})\right)\right], \\
\overline{\delta p q}^{n+1} &= \text{sub-cycled (discussed later)}, \\
\vec{v}_h^{\,n+1} &= \vec{v}_h^{\,n} - \vec{\Gamma}^{1}\left[(\zeta + f)\,\vec{k} \times \vec{v}_h\right] - \nabla_h\left(\vec{\Gamma}^{2}\kappa\right) - \Delta t_{dyn}\widehat{P}, \\
\overline{\Theta \delta p}^{n+1} &= \overline{\Theta \delta p}^{n} + F^{\lambda}\left[\frac{1}{2}\left(\overline{\Theta \delta p}^{n} + f^{\theta}(\overline{\Theta \delta p}^{n})\right)\right] + F^{\theta}\left[\frac{1}{2}\left(\overline{\Theta \delta p}^{n} + f^{\lambda}(\overline{\Theta \delta p}^{n})\right)\right],
\end{aligned}
$$

- No explicit diffusion operators in equations (so far!).
- Implicit diffusion trough monotonicity constraints in F and f operators.
- CAM-FV has 'control' over vorticity at the grid scale through implicit diffusion in the operators F and f but it does not have explicit control over divergence near the grid scale.

Adiabatic frictionless equations of motion

Hydrostatic equations of motion integrated over a Lagrangian layer

$$
\begin{aligned}
\overline{\delta p}^{n+1} &= \overline{\delta p}^{n} + F^{\lambda}\left[\frac{1}{2}\left(\overline{\delta p}^{n} + f^{\theta}(\overline{\delta p}^{n})\right)\right] + F^{\theta}\left[\frac{1}{2}\left(\overline{\delta p}^{n} + f^{\lambda}(\overline{\delta p}^{n})\right)\right], \\
\overline{\delta p q}^{n+1} &= \text{sub-cycled (discussed later)}, \\
\vec{v}_h^{n+1} &= \vec{v}_h^{n} - \vec{\Gamma}^{1}\left[(\zeta + f)\,\vec{k} \times \vec{v}_h\right] - \nabla_h\left(\vec{\Gamma}^{2}\kappa\right) - \Delta t_{dyn}\widehat{P} + \Delta t_{dyn}\nabla_h(\nu D), \\
\overline{\Theta \delta p}^{n+1} &= \overline{\Theta \delta p}^{n} + F^{\lambda}\left[\frac{1}{2}\left(\overline{\Theta \delta p}^{n} + f^{\theta}(\overline{\Theta \delta p}^{n})\right)\right] + F^{\theta}\left[\frac{1}{2}\left(\overline{\Theta \delta p}^{n} + f^{\lambda}(\overline{\Theta \delta p}^{n})\right)\right],
\end{aligned}
$$

- No explicit diffusion operators in equations.
- Implicit diffusion trough monotonicity constraints in F and f operators.
- The above discretization leads to 'control' over vorticity at the grid scale through implicit diffusion but no explicit control over divergence.
- Add divergence damping term to momentum equations.

  Divergence damping uses explicit time-stepping; model will be unstable for too large divergence damping coefficients

Total kinetic energy spectra

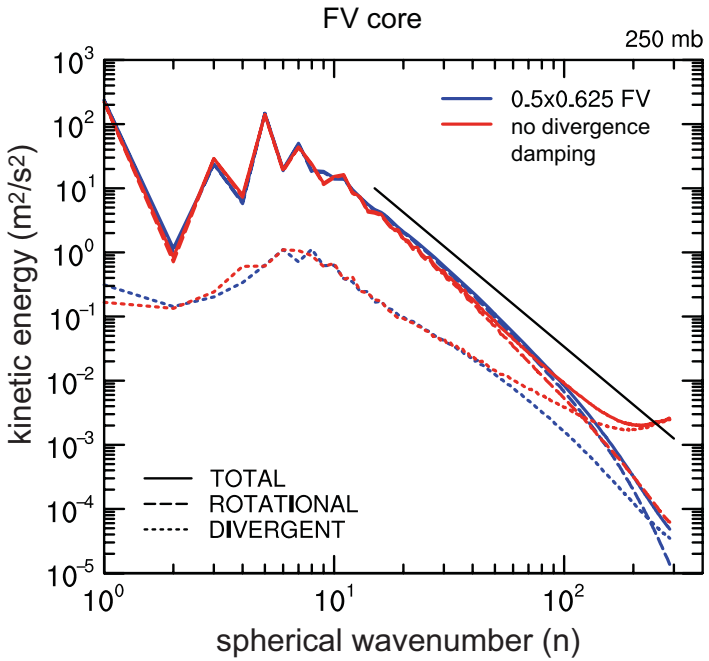

Figure: Solid black line shows k^{-3} slope. Plot courtesy of David L. Williamson.

Without divergence damping there is a spurious accumulation of total kinetic energy associated with divergent modes near the grid scale.

Time-stepping: The 'CD'- grid approach

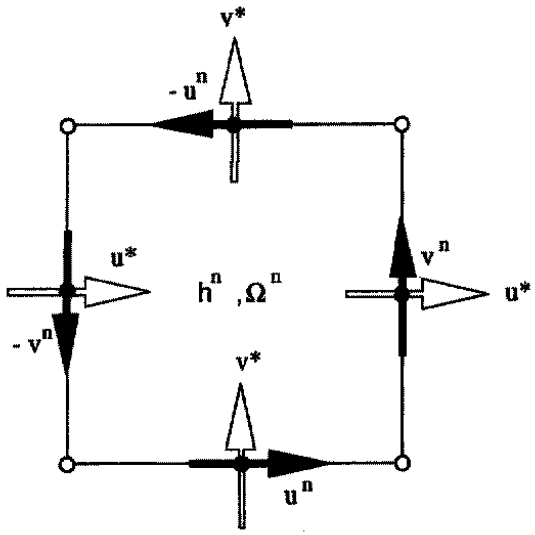

Figure from Lin and Rood (1997).

Definition of Arakawa C and D horizontal staggering (Arakawa and Lamb, 1977):

- C: Velocity components at the center of cell faces and orthogonal to cell faces and mass variables at the cell center. Natural choice for mass-flux computations when using Lin and Rood (1996) scheme.
- D: Velocity components parallel to cell faces and mass variables at the cell center. Natural choice for computing the circulation of vorticity $(\frac{\partial v}{\partial x} - \frac{\partial u}{\partial y})$.

Time-stepping: The 'CD'- grid approach

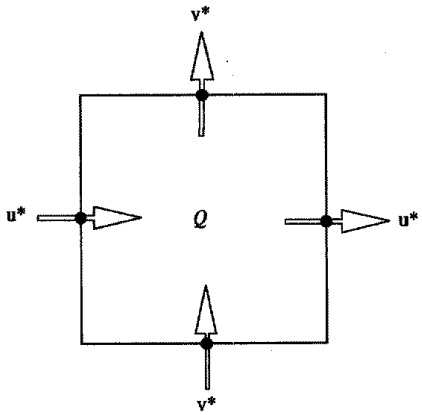

Figure from Lin and Rood (1997).

- For the flux- and advection operators (F and f, respectively) in the Lin and Rood (1996) scheme the time-centered advective winds (u^*, v^*) for the cell faces are needed:
- An option: Extrapolate winds (as in semi-Lagrangian models) $\Rightarrow$ Noise near steep topography (Lin and Rood, 1997).

- Instead, the equations of motion are integrated forward in time for $\frac{1}{2}\Delta t_{dyn}$ using a C grid horizontal staggering.
- These C-grid winds (u^*, v^*) are then used for the 'full' time-step update (everything else from the C-grid forecast is 'thrown away').
- The 'full' time-step update is performed on a D-grid.
- For a linear stability analysis of the 'CD'-grid approach see Skamarock (2008).

Vertical remapping

- CAM-FV uses a Lagrangian ('floating') vertical coordinate ς.
- ς is retained *ksplit* dynamics time-steps Δt_{dyn}.
- Hereafter the prognostic variables are remapped to the Eulerian vertical grid η (the vertical remapping is performed using an energy conserving method, see Lin 2004).
- *ksplit* is set in `namelist`:

`-nsplit` *ksplit*

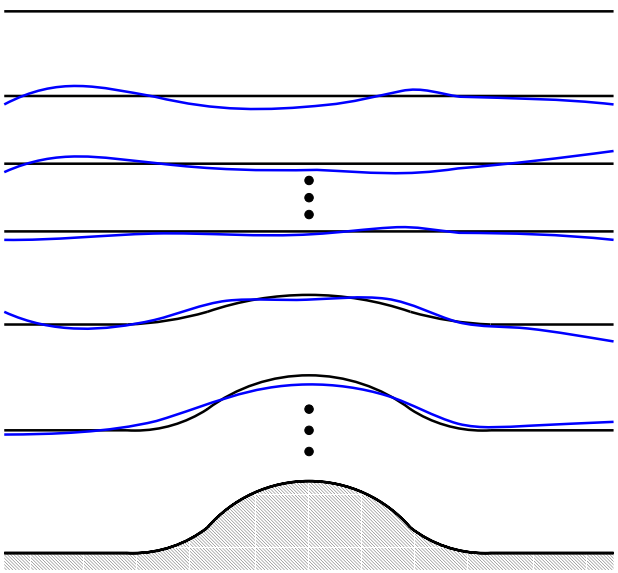

- The 'physics time-step is set in the `namelist`:

`-dtime` Δt,

where Δt s is given in seconds.

- At every physics time-step Δt the variables are remapped in the vertical as described above.
- So the dynamics time-step Δt_{dyn} is controlled with *ksplit* and Δt in the `namelist`:

$$\Delta t = ksplit \times \Delta t_{dyn}.$$

Vertical remapping

- CAM-FV uses a Lagrangian ('floating') vertical coordinate ς.
- ς is retained *ksplit* dynamics time-steps Δt_{dyn}.
- Hereafter the prognostic variables are remapped to the Eulerian vertical grid η (the vertical remapping is performed using an energy conserving method, see Lin 2004).
- *ksplit* is set in `namelist`:

`-nsplit` *ksplit*

- Default setting for the 1.9×2.5 resolution is *ksplit* $= 4$ and $\Delta t = 1800s$ (so $\Delta t_{dyn} = 450s$).
- *ksplit* is usually chosen based on stability.
- (meridians are converging towards the poles) To stabilize the model (and reduce noise) FFT filters are applied along latitudes north and south of the tropics.

Subcycling and tracers

- Continuity equation for air is coupled with momentum and thermodynamic equations:

Subcycling and tracers

- Continuity equation for air is coupled with momentum and thermodynamic equations:
  - thermodynamic variables and other prognostic variables feed back on the velocity field

Subcycling and tracers

- Continuity equation for air is coupled with momentum and thermodynamic equations:
  - thermodynamic variables and other prognostic variables feed back on the velocity field
  - which, in turn, feeds back on the solution to the continuity equation.

Subcycling and tracers

- Continuity equation for air is coupled with momentum and thermodynamic equations:
  - thermodynamic variables and other prognostic variables feed back on the velocity field
  - which, in turn, feeds back on the solution to the continuity equation.
  - Hence the continuity equation for air can not be solved in isolation and one must obey the maximum allowable time-step restrictions imposed by the fastest waves in the system.
- The passive tracer transport equation can be solved in isolation given prescribed winds and air densities, and is therefore not susceptible to the time-step restrictions imposed by the fastest waves in the system.
- For efficiency: Use longer time-step for tracers than for air.

Subcycling and tracers

- Continuity equation for air is coupled with momentum and thermodynamic equations:
  - thermodynamic variables and other prognostic variables feed back on the velocity field
  - which, in turn, feeds back on the solution to the continuity equation.
  - Hence the continuity equation for air can not be solved in isolation and one must obey the maximum allowable time-step restrictions imposed by the fastest waves in the system.
- The passive tracer transport equation can be solved in isolation given prescribed winds and air densities, and is therefore not susceptible to the time-step restrictions imposed by the fastest waves in the system.
- For efficiency: Use longer time-step for tracers than for air.

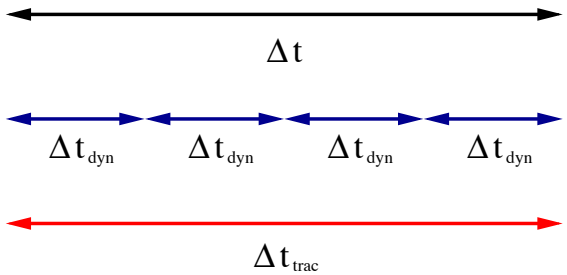

Δt_{trac} is time-step of the tracers. Specified in terms of `nspltrac` (default for 1.9×2.5 resolution is `nspltrac`=1).

Leads to a major 'speed-up' of dynamics.

Free-stream preserving

Simply solving the tracer continuity equation for $\overline{q\delta p}^{n+1}$ using Δt_{trac} will lead to inconsistencies. Why?

Continuity equation for air δp

$$\frac{\partial \delta p}{\partial t} + \nabla \cdot (\delta p \, \vec{v}_h) = 0, \tag{7}$$

and a tracer with mixing ratio q

$$\frac{\partial (\delta p \, q)}{\partial t} + \nabla \cdot (\delta p \, q \, \vec{v}_h) = 0, \tag{8}$$

For $q = 1$ equation (8) reduces to (7). If this is satisfied in the numerical discretizations, the scheme is 'free-stream' preserving.

Solving (8) with $q = 1$ using Δt_{trac} will NOT produce the same solution as solving (7) `nspltrac` times using Δt_{dyn}!

Graphical illustration of 'free stream' preserving transport of tracers

Assume no flux through east cell wall.

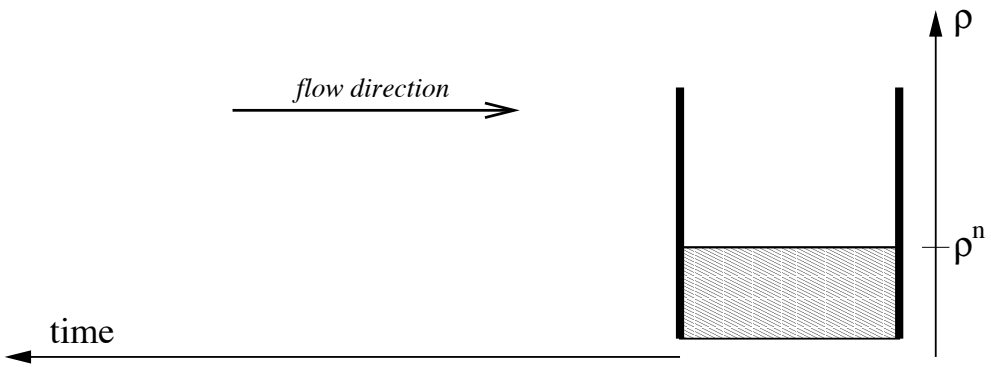

- Solve continuity equation for air $\rho = \delta p$ together with momentum and thermodynamics equations.

Graphical illustration of 'free stream' preserving transport of tracers

Assume no flux through east cell wall.

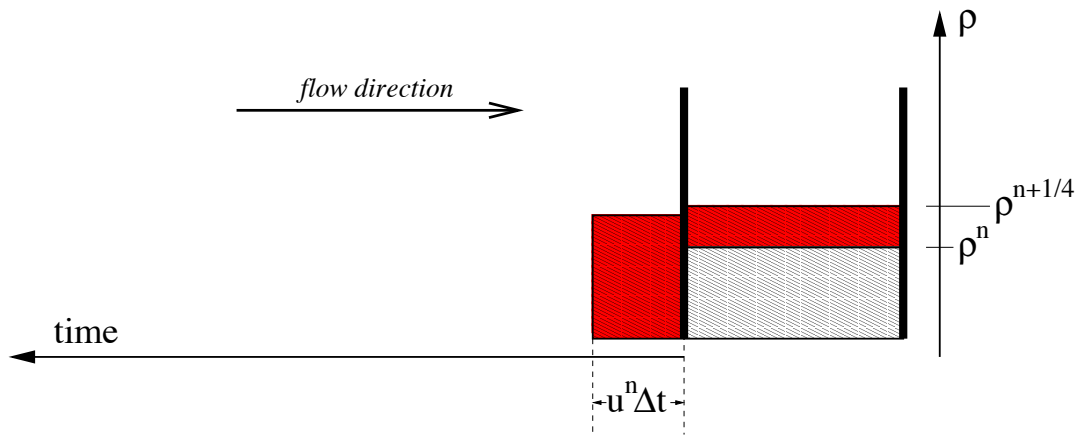

- Solve continuity equation for air $\rho = \delta p$ together with momentum and thermodynamics equations.

Graphical illustration of 'free stream' preserving transport of tracers

Assume no flux through east cell wall.

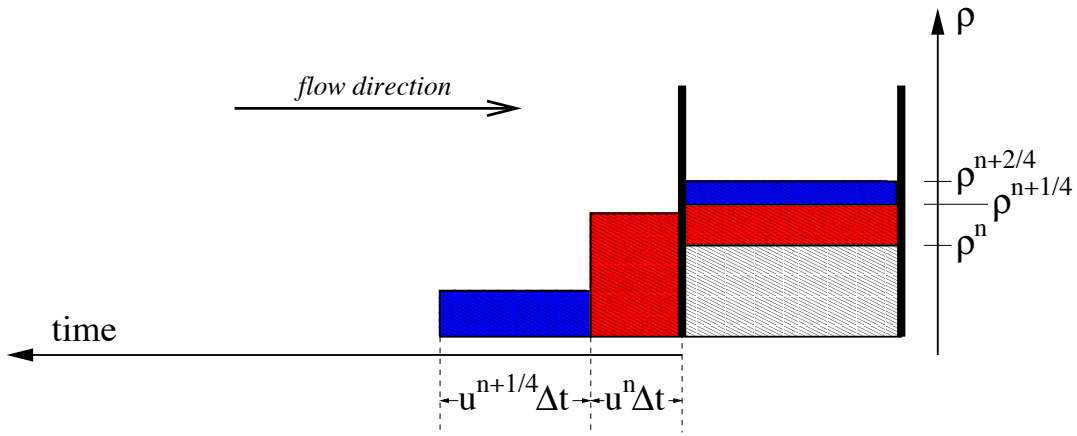

- Solve continuity equation for air $\rho = \delta p$ together with momentum and thermodynamics equations.
- Repeat *ksplit* times

Graphical illustration of 'free stream' preserving transport of tracers

Assume no flux through east cell wall.

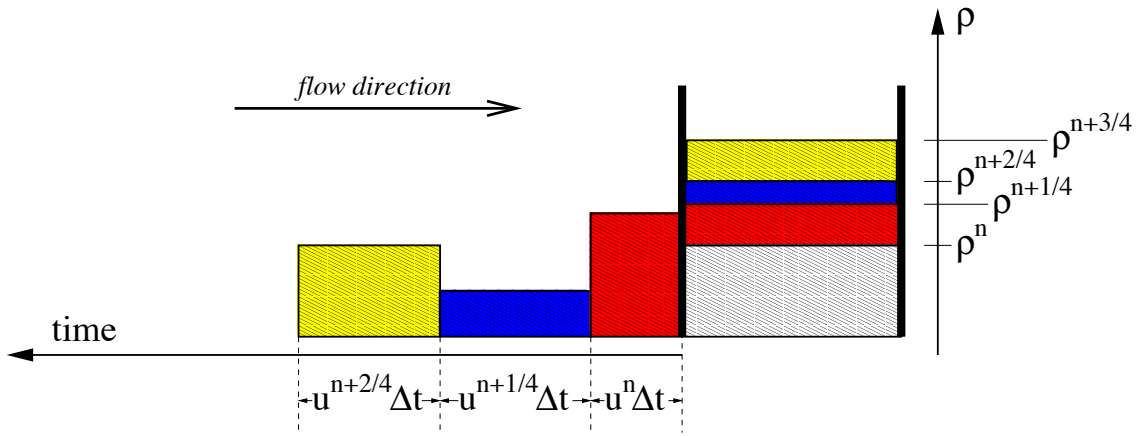

- Solve continuity equation for air $\rho = \delta p$ together with momentum and thermodynamics equations.
- Repeat *ksplit* times

Graphical illustration of 'free stream' preserving transport of tracers

Assume no flux through east cell wall.

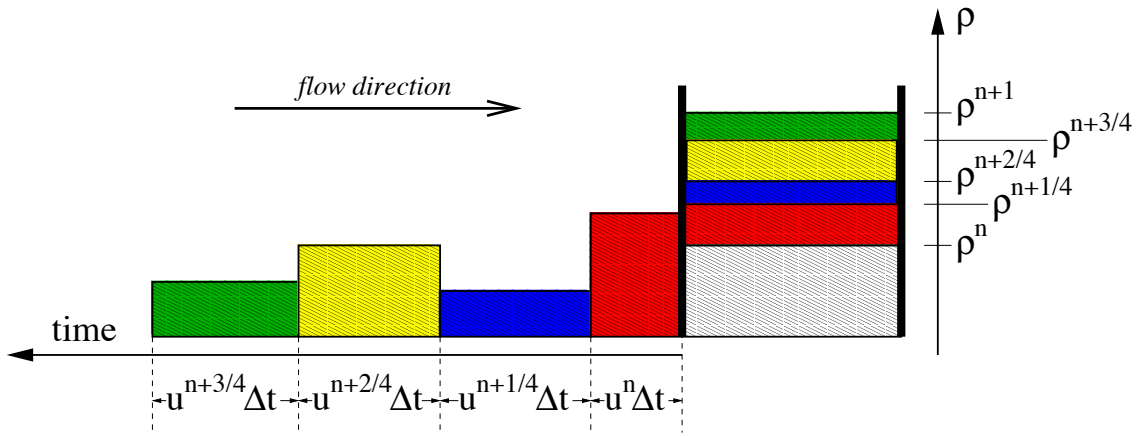

- Solve continuity equation for air $\rho = \delta p$ together with momentum and thermodynamics equations.
- Repeat *ksplit* times

Graphical illustration of 'free stream' preserving transport of tracers

Assume no flux through east cell wall.

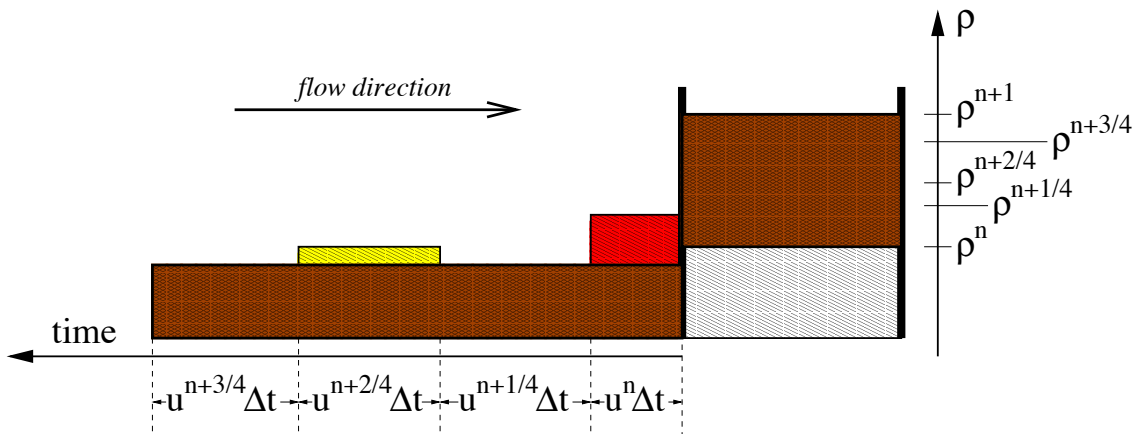

- Solve continuity equation for air $\rho = \delta p$ together with momentum and thermodynamics equations.
- Repeat *ksplit* times
- Brown area = average flow of mass through cell face.
- Compute time-averaged value of q across brown area using Lin and Rood (1996) scheme: $\overline{\overline{< q >}}$.
- Forecast for tracer is: $\overline{\overline{< q >}} \times \sum_{i=1}^{ksplit} \delta p^{n+i/ksplit}$

CAM-FV's advantage over other CAM dynamical cores

- CAM-FV has a very efficient and quite consistent treatment of the tracers.
- This is very important: Number of trace species in climate models are increasing and accounts for most of the computational 'work' in the dynamical core.

CAM-FV's advantage over other CAM dynamical cores

- CAM-FV has a very efficient and quite consistent treatment of the tracers.
- This is very important: Number of trace species in climate models are increasing and accounts for most of the computational 'work' in the dynamical core.
- Rasch et al. (2006) did a comprehensive study of the characteristics of atmospheric transport using three dynamical cores in CAM (CAM-FV, CAM-EUL, CAM-SL; acronyms defined later):

  The results from this study favor use of the CAM-FV core for tracer transport. Unlike the others, CAM-FV

  - is inherently conservative
  - less diffusive (e.g. maintains strong gradients better)
  - maintains the nonlinear relationships among variables required by thermodynamic and mass conservation constraints more accurately.

CAM-FV's advantage over other CAM dynamical cores

- CAM-FV has a very efficient and quite consistent treatment of the tracers.
- This is very important: Number of trace species in climate models are increasing and accounts for most of the computational 'work' in the dynamical core.
- Rasch et al. (2006) did a comprehensive study of the characteristics of atmospheric transport using three dynamical cores in CAM (CAM-FV, CAM-EUL, CAM-SL; acronyms defined later):

  The results from this study favor use of the CAM-FV core for tracer transport. Unlike the others, CAM-FV

  - is inherently conservative
  - less diffusive (e.g. maintains strong gradients better)
  - maintains the nonlinear relationships among variables required by thermodynamic and mass conservation constraints more accurately.

However, with respect to 'meteorology' CAM-FV needs higher horizontal resolution to produce results equivalent to those produced using the spectral transform dynamical core in CAM (CAM-EUL). See Williamson (2008) for details.

Excessive polar night jet for increasing resolution

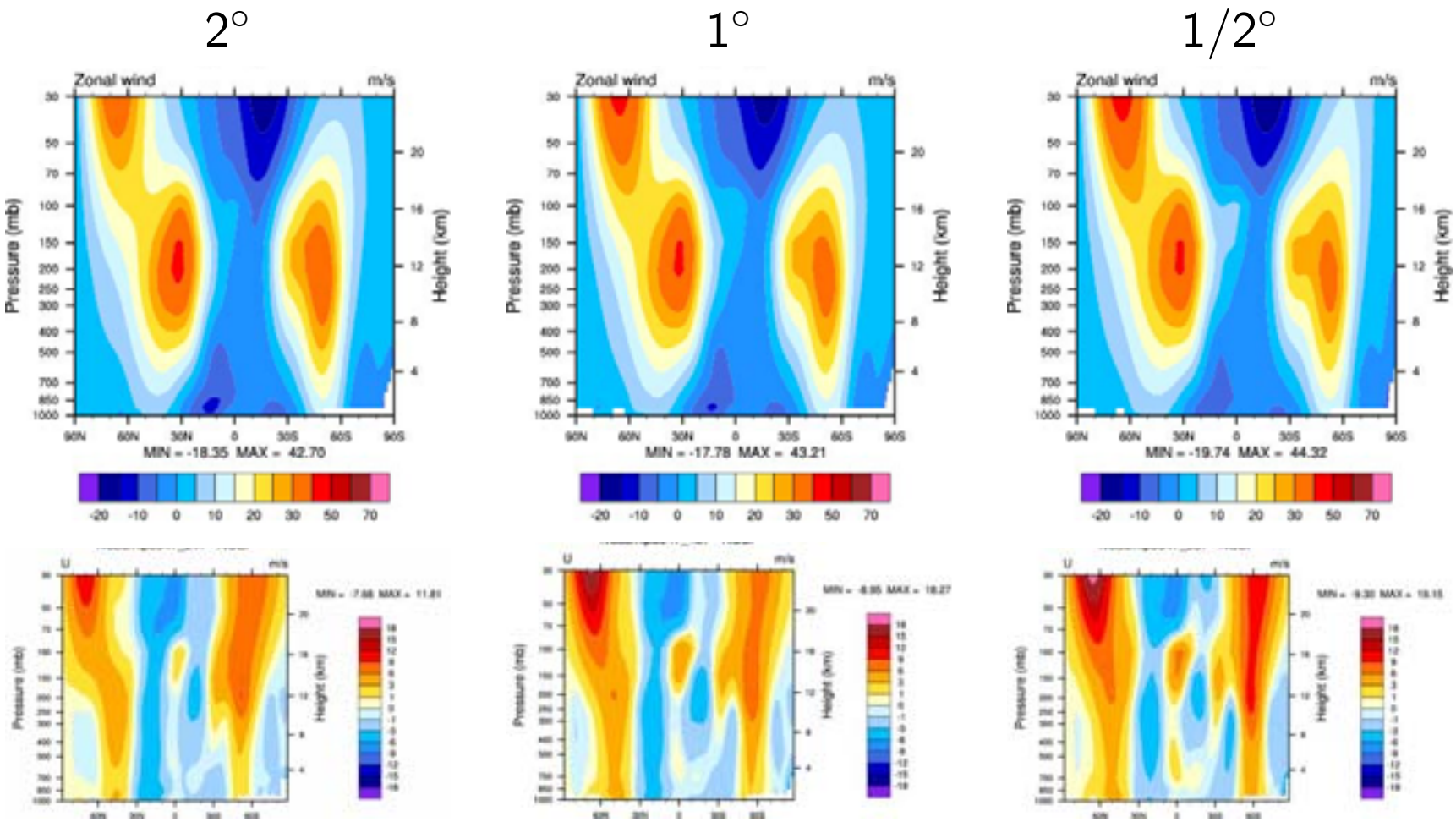

(1st row) Zonally averaged horizontal wind contour plots vs latitude/height from 20-year-averaged AMIP cases. (2nd row) Difference plots using NCEP reanalysis. Plots curtesy of Art Mirin.

Noise in divergence field aligned with grid

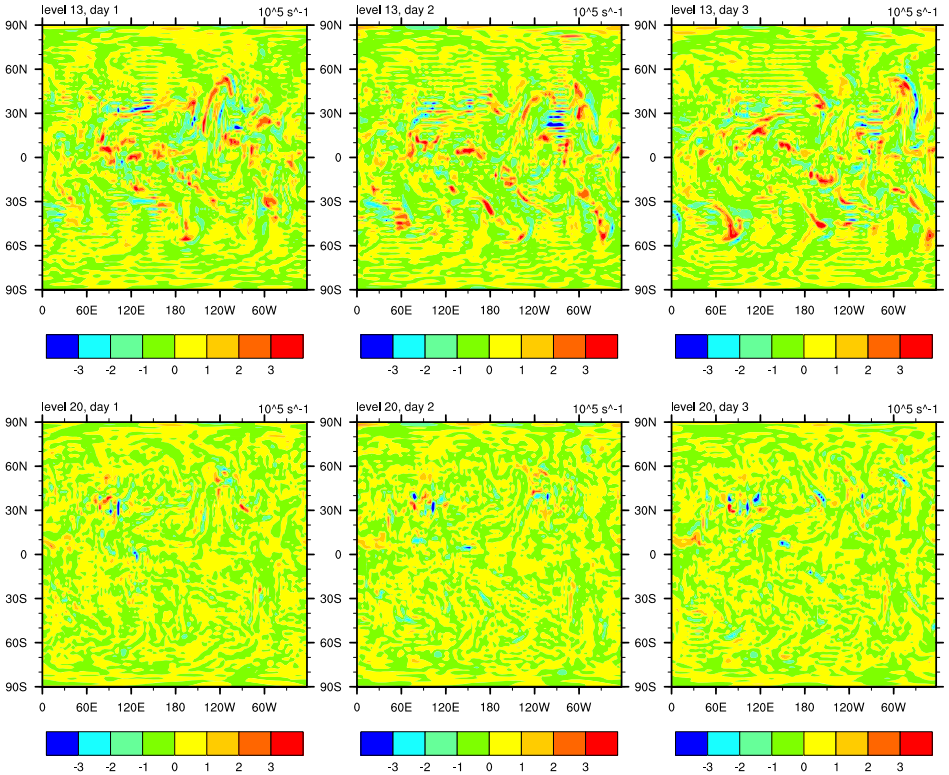

Divergence at model level 13 (first row) and 20 (second row) at days 1,2,3 (left,center,right column), respectively.

The noise can be reduced by increasing the divergence damping coefficient (at the cost of excessive damping in terms of total kinetic energy spectra analysis) or using high-order divergence damping (work in progress).

Noise problems

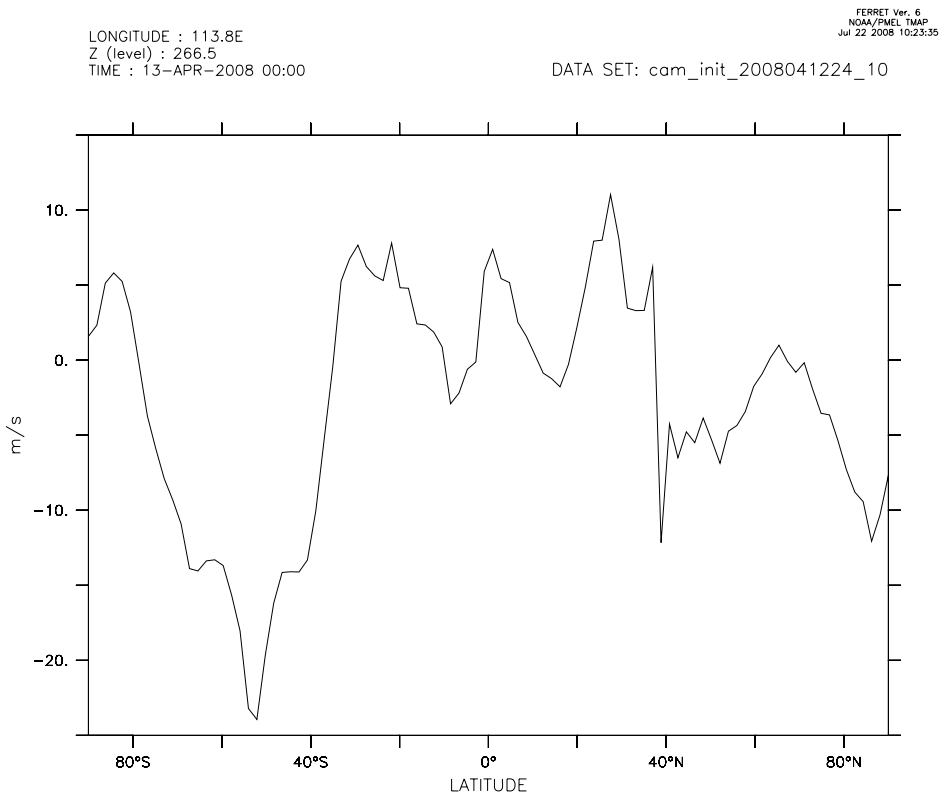

Meridional wind, staggered (m/s)

Sporadic noise is visible occasionally in the meridional wind at upper levels in CAM (noise was first detected 9 months into the simulation).

Idealized settings for CAM

- `ADIABATIC`: No physics. See example of application in Jablonowski and Williamson (2006).
- `IDEAL_PHYS`: Held-Suarez test case (Held and Suarez, 1994):
  - Simple Newtonian relaxation of the temperature field to a zonally symmetric state
  - Rayleigh damping of low-level winds representing boundary-layer friction
- `AQUA_PLANET`: Ocean only planet with zonally symmetric SST-forcing using 'full' physics package (Neale and Hoskins, 2000). See example of application in Williamson (2008).

Other dynamical core options in CAM

- CAM-EUL (Collins et al., 2004):
  - Based on the spectral transform method
  - Semi-implicit time-stepping
  - Tracer transport with non-conservative semi-Lagrangian scheme ('fixers' restore formal mass-conservation)
- CAM-SL (Collins et al., 2004): Same as CAM-EUL but based entirely on a semi-Lagrangian discretization (Collins et al., 2004).
- CAM-HOMME (High-Order Method Modeling Environment, Thomas and Loft 2005):
  - Based on local spectral element method
  - For each element: Mass-conservative to machine precision and total energy conservative to the truncation error of the time integration scheme
  - Discretized on cubed-sphere
  - Highly scalable!
  - Currently being tested in 'AMIP mode' (Contact Mark Taylor for details).

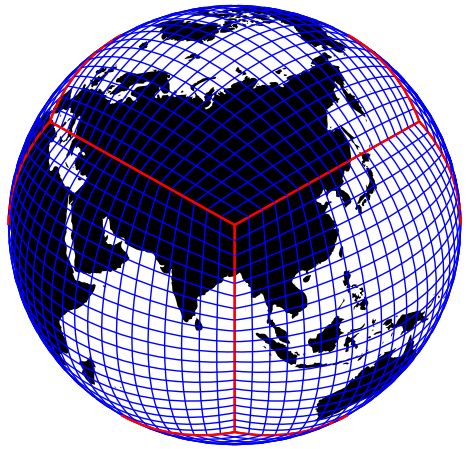

References I

Arakawa, A. and Lamb, V. (1977). Computational design and the basic dynamical processes of the UCLA general circulation model. *Methods in Computational Physics*, 17:173–265.

Colella, P. and Woodward, P. R. (1984). The piecewise parabolic method (PPM) for gas-dynamical simulations. *J. Comput. Phys.*, 54:174–201.

Collins, W. D., Rasch, P. J., Boville, B. A., Hack, J. J., McCaa, J. R., Williamson, D. L., Kiehl, J. T., and Briegleb, B. (2004). Description of the NCAR Community Atmosphere Model (CAM 3.0). NCAR Tech. Note, NCAR/TN-464+STR.

Godunov, S. (1959). A difference scheme for numerical computation of discontinuous solutions of equations in fluid dynamics. *Math. Sb.*, 47:271. Also: Cornell Aero. Lab. translation.

Held, I. M. and Suarez, M. J. (1994). A proposal for the intercomparison of the dynamical cores of atmospheric general circulation models. *Bull. Amer. Meteor. Soc.*, 75:1825–1830.

Jablonowski, C. and Williamson, D. L. (2006). A baroclinic instability test case for atmospheric model dynamical cores. *Q. J. R. Meteorol. Soc.*, 132:2943–2975.

Lauritzen, P. H. (2007). A stability analysis of finite-volume advection schemes permitting long time steps. *Mon. Wea. Rev.*, 135:2658–2673.

Lin, S. (1997). Ti: A finite-volume integration method for computing pressure gradient force in general vertical coordinates. *Quart. J. Roy. Meteor. Soc.*, 123:1749–1762.

Lin, S. and Rood, R. (1996). Multidimensional flux-form semi-Lagrangian transport schemes. *Mon. Wea. Rev.*, 124:2046–2070.

Lin, S.-J. (2004). A 'vertically Lagrangian' finite-volume dynamical core for global models. *Mon. Wea. Rev.*, 132:2293–2307.

Lin, S.-J. and Rood, R. (1997). An explicit flux-form semi-Lagrangian shallow-water model on the sphere. *Q.J.R.Meteorol.Soc.*, 123:2477–2498.

Machenhauer, B., Kaas, E., and Lauritzen, P. H. (2009). Finite volume methods in meteorology, in: R. Temam, J. Tribbia, P. Ciarlet (Eds.), Computational methods for the atmosphere and the oceans. *Handbook of Numerical Analysis*, 14. Elsevier, 2009, pp.3-120.

Neale, R. B. and Hoskins, B. (2000). A standard test for AGCMs and their physical parameterizations. i: The proposal. *Atmos. Sci. Letters*, 1:101–107.

References II

Rasch, P., Coleman, D., Mahowald, N., Williamson, D., Lin, S., Boville, B., and Hess, P. (2006). Characteristics of atmospheric transport using three numerical formulations for atmospheric dynamics in a single GCM framework. *J. Climate*, 19:2243–2266.

Skamarock, W. C. (2008). A linear analysis of the NCAR CCSM finite-volume dynamical core. *Mon. Wea. Rev.*, 136:2112–2119.

Thomas, S. and Loft, R. (2005). The NCAR spectral element climate dynamical core: Semi-implicit eulerian formulation. *J. Sci. Comput.*, 25:307–322.

Thuburn, J. (2008). Some conservation issues for the dynamical cores of nwp and climate models. *J. Comput. Phys.*, 227:3715 – 3730.

van Leer, B. (1977). Towards the ultimate conservative difference scheme. IV: A new approach to numerical convection. *J. Comput. Phys.*, 23:276–299.

Williamson, D. L. (2008). Equivalent finite volume and eulerian spectral transform horizontal resolutions established from aqua-planet simulations. *Tellus*, 60:839–847.